[redacted]

DEPARTMENT OF THE AIR FORCE
AIR UNIVERSITY

AIR FORCE INSTITUTE OF TECHNOLOGY

Wright-Patterson Air Force Base, Ohio

AFIT/GNE/ENP/90M-8

INVESTIGATION OF THE EFFECT OF MECHANICAL STRESS ON COLD FUSION

THESIS

Barton H. Wohl
Major, USAF

AFIT/GNE/ENP/90M-8

AFIT/GNE/ENP/90M-8

INVESTIGATION OF THE EFFECT OF MECHANICAL STRESS ON COLD FUSION

THESIS

Presented to the Faculty of the School of Engineering

of the Air Force Institute of Technology

Air University

In Partial fulfillment of the

Requirements for the Degree of

Master of Science

Barton H. Wohl, B.S.

Major, USAF

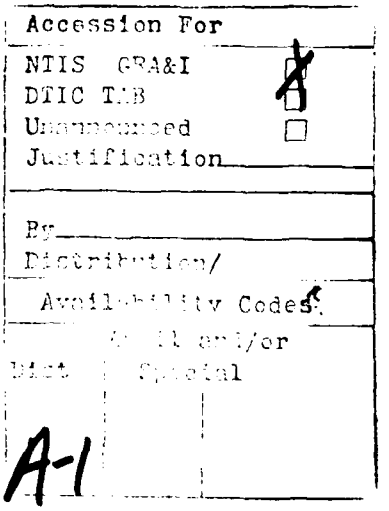

March 1990

Approved for public release; distribution unlimited

Preface

The chance to help prove or disprove cold fusion of deuterium was selected as my thesis topic because it seemed like an exciting fundamental question. What it turned out to be was an intense education in the interdisciplinary nature of nuclear engineering, and science in general. Successful completion of this thesis involved work, design or study in metallurgy, radiation detection, physical chemistry, wet chemistry, solid state physics, metallography, materials testing, and vacuum systems. A little bit of blood and a lot of sweat also helped.

As the excitement of the fundamental question faded, the reward and frustration of interdisciplinary work made themselves known. The details of the frustration are almost forgotten, but the reward was the opportunity to work with many of the talented and dedicated people at Wright-Patterson AFB. The members of my committee, Dr. George John, Maj Denis Beller, and Capt Pete Haaland all shared their knowledge freely with me. Jimmy Ray of the Propulsion Lab lent me critical space and material support. While virtually every member of the AFIT Model Fabrication Branch helped, particular mention must be made of Tim Hancock, who built the bulk of the equipment. Many other people deserve thanks, and I apologize for not listing them here individually.

Work on a thesis is not only done at Wright-Patterson AFB, but also at home. I would like to thank my wife Callista and daughter Devon for their patience and devotion during these long months.

Barton H. Wohl

Table of Contents

List of Figures

List of Tables

Abstract

The purpose of this research was to see if the phenomenon known as "cold fusion" could be observed after loading a sample of titanium with deuterium gas and then subjecting the sample to mechanical stress. Samples of commercially pure titanium were loaded with deuterium by heating them inductively to 643 ± 4° C while they were in a deuterium atmosphere. After loading, the samples were subjected to either dynamic tensile stress, a static load, or shear stress. The samples were surrounded by a 4π neutron detector during the application of stress and data from the detection system was analyzed for either large bursts of neutrons or continous low-level emission of neutrons. Despite the fact that the neutron detection system was sensitive to certain environmental factors, application of tensile stress caused no positive indications of cold fusion. One suspiciously large count did occur during the application of shear stress, but that part of the experiment was relatively uncontrolled, and it is believed that the one large count was caused by environmental factors. An upper limit of 1.2×10^{-24} neutrons/deuteron pair/s has been calculated for the samples involved in this research. This is based on the limits of sensitivity of the neutron detection system.

I. Introduction

Purpose

The purpose of this research was to see if the phenomenon known as "cold fusion" could be observed after loading a sample of titanium (Ti) with deuterium (D) gas and then subjecting the sample to mechanical stress. Cold fusion can be defined as a phenomenon in which some combination of neutrons, excess heat, and tritium is released when a transition metal, such as palladium or titanium, at about room temperature, has absorbed a quantity of deuterium.

Background

In March 1989, M. Fleischmann and S. Pons of the University of Utah surprised the scientific world with the announcement that they had created "cold fusion in a jar." Pons and Fleischmann claimed (1:308) to observe cold fusion in an electrolytic cell containing a palladium cathode, D_2O, and various salts. Shortly thereafter, S. E. Jones et al. at BYU also claimed (2:739) to observe the phenomenon while working with electrolytic cells, but Jones used a titanium cathode as well as palladium.

Deuterium atoms are known to fuse with themselves in the reactions (1:302)

$$D + D \rightarrow T(1.01\ MeV) + p(3.02\ MeV) \tag{1}$$

or

$$D + D \rightarrow {}^{3}He(0.82\ MeV) + n(2.45\ MeV) \tag{2}$$

under conditions of high temperature and pressure. Deuterium-deuterium (DD) fusion is known to occur and become self-sustaining at energies greater than 2.5-KeV (3:17), under conditions like those found in nuclear weapons. What makes Pons and Fleischman's claims exceptionally noteworthy is that, if true, they hold out the promise of cheap energy with no air pollution, no water pollution, and minimal radioactive waste compared to traditional nuclear power plants.

Since Pons and Fleischmann made their announcement, several groups of researchers have attempted to duplicate their work using electrolytic cells. Other groups have searched for cold fusion in environments other than electrolytic cells. Fruitless searches have been conducted in deuterium plasmas generated by glow discharges and RF energy. Neutron bursts significantly greater than background have been reported as titanium chips in high pressure D_2 gas (4) warmed up to room temperature after repeated immersion in liquid nitrogen and also in D_2 gas where both temperature and pressure were varied in a controlled manner (5:221). A possible implication of neutron bursts during warming is that thermal or mechanical stress has a role in cold fusion.

Scope of the Project

This project required development of several procedures and pieces of equipment. The process of deuteriding titanium required the construction of a vacuum system and the design of a protocol for cleaning the titanium samples, loading them with deuterium, and calculating the deuterium uptake in the samples. Once the samples were loaded with deu-

terium, mechanical stress was applied while the samples were surrounded by a 4π neutron detector, which was designed, tested, and calibrated specifically for this project.

Since stress was applied to the samples while they were surrounded by a 4π neutron detector, miniature grips were designed to hold the samples during the individual trials. Procedures were developed to place the deuterided samples in the grips, place the gripping assembly in the neutron detector, and then apply stress to the samples.

In addition to the equipment and procedures already mentioned, metallurgical analysis was performed in order to characterize the samples. A clean titanium sample and a deuterided titanium sample were examined with optical metallography. Fracture surfaces from two of the stressed samples were examined with a scanning electron microscope.

Plan of the Report

Section II of the report briefly reviews the Ti-Hydrogen system, using the Ti-H phase diagram as a reference. After the discussion of Ti-H, two different theories of cold fusion are addressed. The first theory involves segregation of deuterium at locations of stress in a metal, and the second theory is the crack-induced particle accelerator theory.

Theory is followed by a section on the design of the experiment. This section includes discussion of the selected methods and sources of experimental uncertainty. Also included in this section are details of the apparatus and experimental procedures used to load titanium samples with deuterium, apply stress to the samples, measure any neutron output

from the samples, and characterize the samples metallographically.

Section IV, Results and Discussion, compares the results of the experimental trials with the results of the background counts described in Section III. In addition, an upper limit on cold fusion neutrons is determined, based upon the sensitivity of the neutron detector.

Conclusions and recommendations are presented in Section V. The conclusions are drawn directly from Section IV. If there is still interest in the subject, the recommendations suggest ways to follow-up on this work in the future.

II. Theory

Two hypotheses have been advanced that relate mechanical stress to cold fusion. A very brief discussion of the Ti-Hydrogen (H) system will lay a foundation for review of the hypotheses. Ti-H is the system being reviewed because of a scarcity of literature on the Ti-D system.

Ti-H System

Hydrogen, upon encountering an oxide-free Ti surface (6:465), will readily dissociate into atomic form and diffuse into the metal. The individual H atoms will diffuse through the metal in an interstitial solution while the concentration of H remains low. This can be seen in the Ti-H phase diagram, reproduced in Fig. 1. H has a maximum solubility of 6.72 atomic percent in hexagonal close-packed α-phase Ti, at a temperature of 300° C. Above 300° C, H has a maximum solubility of about 50 atomic percent in body centered cubic β-phase Ti, at a temperature of 720° C.

Further review of the phase diagram shows that if a piece of Ti is heated to the temperature range above 300° C while exposed to a D_2 atmosphere, the Ti will absorb an amount of hydrogen determined by the solubility of H in the β-phase. In reality, it is necessary to heat Ti above 400° C to dissolve a surface oxide layer and enable H to enter the metal (6:466). When the source of heat is removed, a hydride will precipitate out of the supersaturated α-phase as the α-phase forms. Upon cooling to room temperature, the piece of Ti will consist of a mixture of α-phase with H in solution, titanium hydride, and some β-phase with H

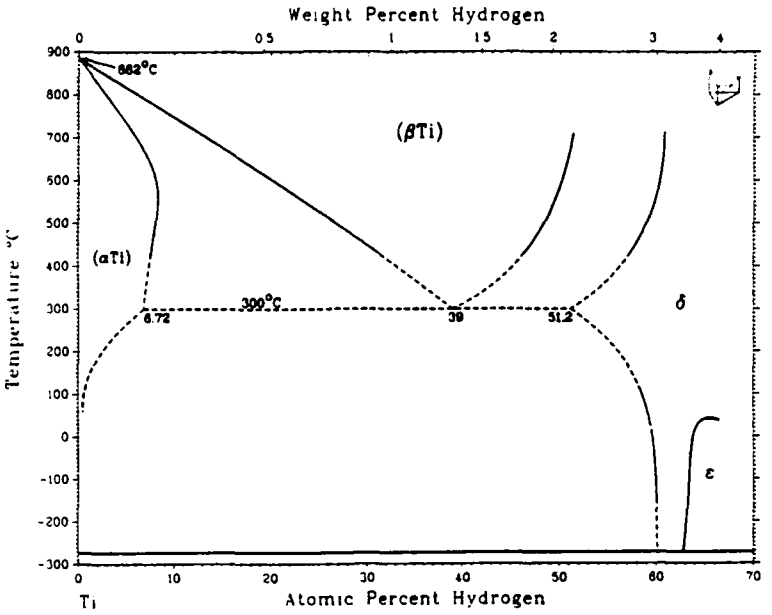

Fig. 1. Ti-H Phase Diagram(7:1284)

in solution. The β-phase will exist if the sample cooled more rapidly than the transition between phases could occur, and is known as "retained β."

Cold Fusion

As mentioned previously, mechanical stress is a factor in two hypotheses that have been advanced as possible explanations of cold fusion. The first hypothesis involves segregation of hydrogen at regions of stress. The second involves crack-generated particle acceleration.

Hydrogen accumulates at regions of stress in metals. It may precipitate to grain boundaries or dislocations (8:105). Phase interfaces in Ti can also form high local concentrations of hydrogen (9:1233). A "hydrogen cloud" forms in the plastic zone ahead of advancing cracks in

Ti (10:419). J. Gittus and J. Bockris (8:105) propose that when local concentrations build to a high enough, but as yet unspecified, level, cold fusion can occur.

Mechanical stress causes both dislocations and cracks in Ti. In addition to creating high local concentrations of hydrogen, cracks may act like particle acelerators when they occur, according to E. J. Mayer et al. (11:25). This supposed phenomenon would be a manifestation of the piezoelectric effect. The piezoelectric effect, or piezoelectricity, is defined as "electric polarization produced by mechanical strain in crystals belonging to certain classes" (12:4). Mechanical strain causes positive charges to go one way in the crystal, while negative charges go the other. This effect causes local charge imbalances of opposite signs on opposite sides of a growing crack. The result would be the creation of an electric field that might be capable of accelerating deuterons to the energies needed for conventional fusion. B. V. Derjaguin et al. suggest that electric fields of up to 10^7 V/cm can be created by destruction of the TiD crystal lattice (13:492).

While the piezoelectric particle accelerator sounds interesting, two cautions must be noted. First, most metals, with very few exceptions do not display the piezoelectric effect (12:9). Second, E. J. Mayer et al. cautioned, at the same time they presented their particle accelerator model, that the piezoelectric effect could generate heat in the metal lattice and be responsible for claimed observations of excess heat (11:25).

Some very simple calculations tend to discredit the piezoelectric effect as a driving force for cold fusion or as a source of excess heat. The D-D coulomb barrier can be shown to be approximately 0.29-MeV, and if the 10^7 V/cm field suggested by Derjaguin et al. stays constant, without discharging like a capacitor, then a deuteron could be accelerated to an energy of 0.29-MeV over a distance of 0.029 cm. If the field decreases in a capacitor-like fashion, then this distance must increase since the field is weakening during the discharge. However, atomic spacings are on the order of angstroms, and 0.029 cm is six orders of magnitude larger. Microcracks should start to form across distances comparable to atomic spacing in a brittle material like TiD. There does not appear to be enough distance for a deuteron to accelerate across a crack and achieve 0.29-MeV of kinetic energy.

The piezoelectric effect also does not appear to be a good source of excess heat. Using an infinite parallel-plate capacitor model, the electrostatic energy between both sides of a microcrack is given below (14:59):

$$W = \frac{1}{2}\int \epsilon E^2 dV \qquad (3)$$

With an $\vec{E}$ field of 10^7 V/cm and microcracks, about 1" long and 0.05" wide, as found in the samples used in this investigation, the electrostatic energy, as given by the above equation, is about 10^{-12} joules. This small amount of energy will not perceptibly raise the temperature of titanium or a beaker of heavy water.

III. Design of the Experiment

Method Used

Four samples of titanium were loaded with deuterium by inductively heating them to 643° C in one atmosphere of D_2 gas. Three of the four samples were then mechanically stressed. The first sample, while surrounded by a 4π neutron detector, was subjected to tensile stress at a speed of 0.1 inches/minute until failure in an Instron 20,000 pound materials testing machine (Hereafter referred to as "the Instron"). A relatively slow speed was selected in order to increase integration time. Shear stress was then applied to the first and second samples using a pair of $12\frac{1}{2}$-inch-long household shears. The third sample was placed in tension for 30 minutes with a static load of 50 pounds. In order to characterize the deuterided titanium, the fourth sample was reserved for metallographic analysis.

Sources of Uncertainty

As a test of whether or not mechanical stress can induce cold fusion in deuterided titanium, there were several sources of uncertainty in this research. The first resides in the titanium samples themselves. They were commercially pure, and a microscopic x-ray fluorescence analysis revealed the following composition (percentages by weight):

Aluminum - 0.42%

Titanium - 99.29%

Manganese - 0.004%

Iron - 0.24%

Nickel - 0.004%

Zirconium - 0.01%

Niobium - 0.02%

Molybdenum - 0.005%

The trace elements could have an effect on the cold fusion process, either as catalysts or inhibitors (15).

Another source of uncertainty also deals with the purity of the samples, or in this case, the surface of the samples. Because of the nature of the experiment and time restrictions, it was deemed impossible to keep the samples in a D_2 atmosphere for the entire procedure. Instead, the samples were removed from the D_2 after loading, and exposed to air until stress was applied. There is still debate as to whether observed cold fusion effects are surface or bulk effects. If it's a surface effect, air could also affect the process.

A third source of uncertainty was the sensitivity of the neutron detection system to environmental influences, such as turning lights on or hitting the inner lining. This sensitivity would tend to generate false positive results that must be carefully weeded out.

A possible minor source of uncertainty is the rate at which stress was applied to the samples. The ductility of mildly hydrided (on the order of hundreds of ppm) titanium varies in part with the rate at which stress is applied (16:1). The samples used in this research were deuterided to tens of thousands of ppm and appeared to be equally brittle at any stress rate. There was, however, no time available to confirm this in detail.

Procedure and Apparatus

Details of the Apparatus.

Vacuum Apparatus. Loading of the Ti samples with deuterium occurred in a portable vacuum apparatus, shown in Fig. 2. The major components of the apparatus are a diaphragm pump, molecular drag pump, 30 liter/s triode ion pump and controller, manifold, a capacitance manometer with a 1000-torr range, and two bellows valves. All of the components except for the diaphragm pump were placed or mounted on a cart with a 24" x 30" wooden base and an upright frame made from Unistrut building material.

The manifold contained an 8-inch-long, 1.375-inch-diameter quartz and graded-glass chamber, a Varian 4-way cross, a Varian tee, and the 1/4 inch stainless steel tubing necessary to connect the capacitance manometer to the system. One bellows valve separated the manifold from the ion pump and the other bellows valve separated the drag pump from the manifold. Both bellows valves and the manifold components, except the quartz chamber, were cleaned ultrasonically in a solution of Alconox detergent and water, rinsed with deionized water, rinsed with dichloromethane, given a final rinse with deionized water, and then air-dried.

In addition to the major components described in the preceding paragraphs, a miniature ion pump was attached to the reference side of the manometer and was used both to pump down and to monitor the pressure of the reference side. A 4-way pipe thread cross at the vent of the drag pump provided a place to insert a thermocouple vacuum gauge into the system, a vent to air, and the connection between the diaphragm pump and

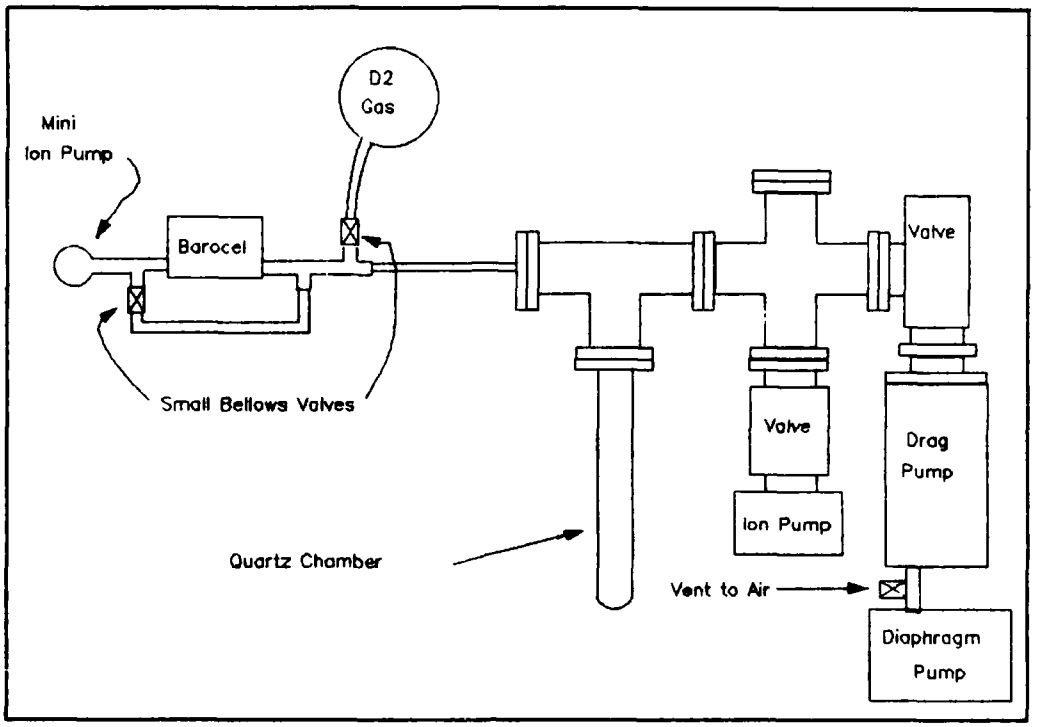

Fig. 2. Schematic of Vacuum Apparatus

the drag pump.

Induction Heater. The induction heater was a model Lepel T2.5-1-KC-AP-BW with a Lepel RWAG-5 heat exchanger. The coil used in this experiment had six turns spread over a $2\frac{1}{16}$-inch length and an inner diameter of $1\frac{15}{16}$ inches.

Materials Testing Machine and Grips. The load cell used in this experiment was an Instron 20,000 pound cell. A pen plotter was used to record the load applied to the titanium samples.

The grips used to hold the deuterided titanium samples in the load cell are shown in Fig. 3. The author designed the grips with two independent jaws as shown in the figure. As tensile stress is applied to a sample, the jaws will try to slide with the sample, be compressed by the

surrounding cylinder, and effectively self-tighten. The AFIT model fabrication branch constructed the jaws out of type 4340 carbon steel. The grips are attached to steel shafts that were held in place in the materials testing machine with 3/8-inch steel pins.

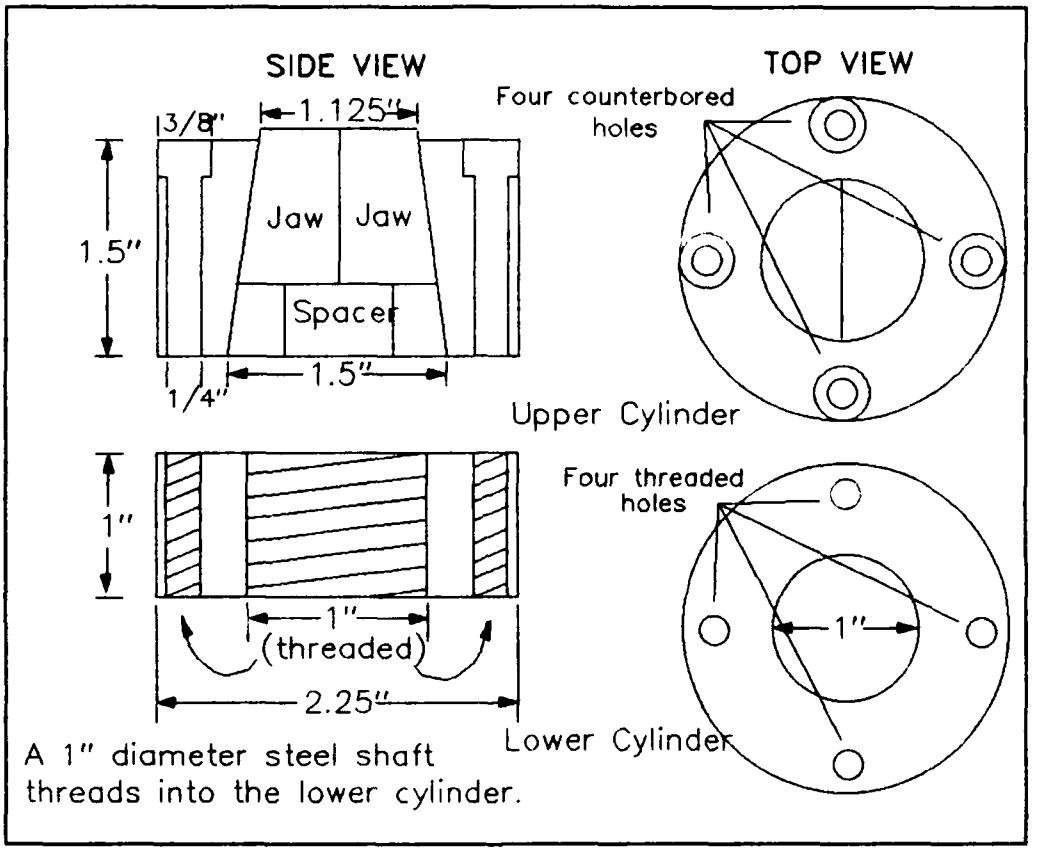

Fig. 3. Grips

Neutron Detector.

Hardware. The 4π neutron detector, shown in Fig. 4, consists of six cylindrical detectors that are 1" in outer diameter and 14" in total length with a sensitive region that is 12" long. These tubes are filled with ^{3}He at a pressure of 4 atmospheres. To enhance their efficiency for counting fast neutrons, they are placed in a cylindrical

polyethylene moderator in a circular array around the axis of the moderator. The detectors are inserted so that they are centered lengthwise in the moderator.

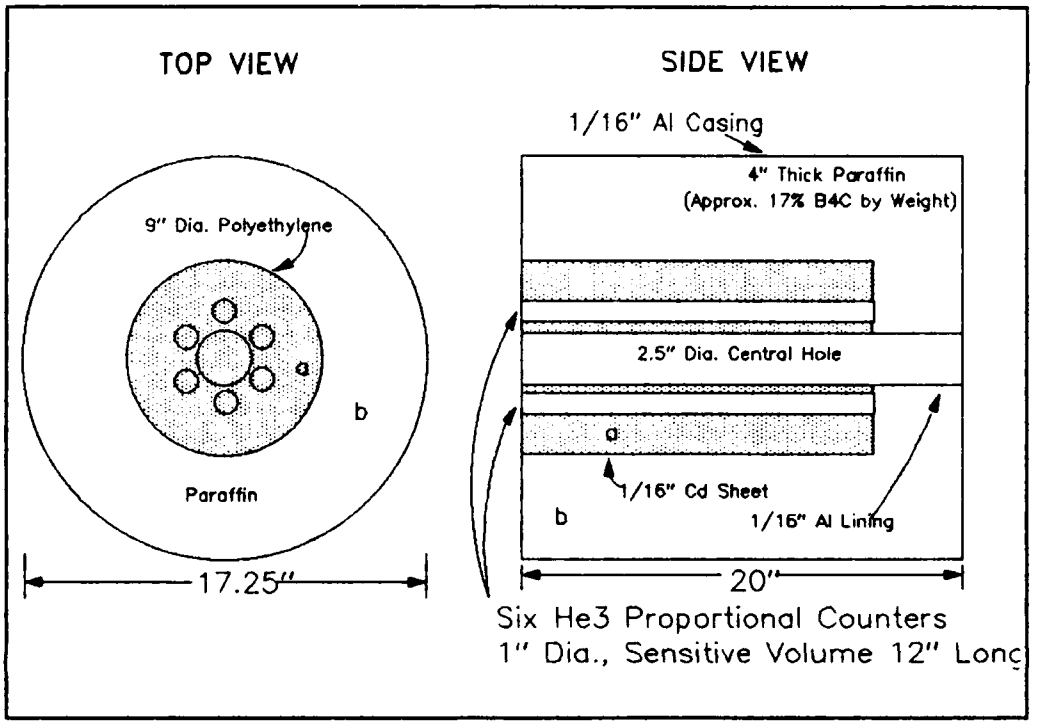

Fig. 4. 4π Neutron Detector

The moderator is a high-density polyethylene cylinder that is 16" long and 9" in diameter. The center of the cylinder is bored to contain an aluminum tube that has an inner diameter of 2.5" and a wall thickness of 1/16." Only 1/16" of polyethylene separates the ^{3}He detectors from the aluminum lining of the central chamber, in order to have the ^{3}He detectors as close to the central chamber as possible, thereby maximizing the efficiency of the 4π detector (17:182).

The moderator is encased in three more layers. The first layer is a 1/16" thick cadmium sheet. Surrounding the cadmium is a 4" layer of paraffin, with approximately 17% B_4C by weight. A 1/16" thick sheet of aluminum encloses all but the face of the detector.

The output signals from all six ^3He detectors are fed to a small electrical chassis, in which the six coaxial cables, carrying the signals, are connected in parallel. One cable then connects the chassis to a single preamplifier. The operating bias chosen for this experiment, +1200V, is provided by one power supply to the six detectors via the one preamplifier and chassis (See Fig. 5).

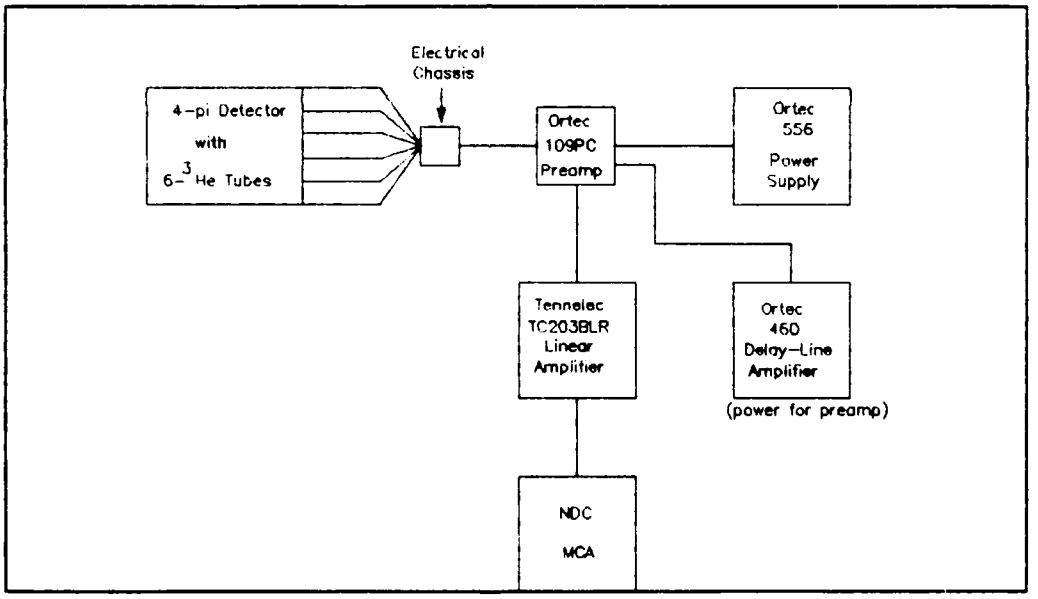

Fig. 5. Electronic Modules in Neutron Detection System

From the preamplifier, signals were fed to a linear amplifier and then to a Nuclear Data multichannel analyzer (MCA). The MCA ran Nuclear Data's AccuSpec program on a Zenith Z248 PC which contained an AccuSpec expansion board. The MCA was operated in multi-scale mode.

Estimation of Efficiency. The efficiency of the neutron detector was measured experimentally by using a PuBe source of known strength, and it was calculated for 2.45-MeV neutrons from the DD reaction by using MORSE (18), a Monte Carlo radiation transport code.

In an effort to avoid saturating the 4π detector when measuring its efficiency, the least active available PuBe source, T022, was used to measure efficiency. The neutron output of T022 was determined by making separate counts with a long counter of a stronger, known, source (M1170) and T022, under identical conditions. The ratio of the two counts indicated that T022 emitted $(1.23 \pm 0.07) \times 10^5$ neutrons/second.

The 4π neutron detection system recorded 1,440,159 counts in 100 seconds with T022 suspended in the middle of the polyethylene cylinder. After accounting for a background count of 903 counts in 1054.1 seconds, the measured efficiency of the detector for a PuBe source was 0.117 ± 0.006. However, many apparently simultaneous pulses were observed while monitoring the output of the linear amplifier during the 100-second count with T022. This necessitated a correction to the efficiency, and it was made with an equivalent deadtime correction of 4.9-μs. This correction yielded a new value for the upper limit of measured efficiency of approximately 0.13 (See Appendix A).

To estimate the efficiency of the detection system for 2.45-MeV DD neutrons, MORSE was run for two cases. The first case was a PuBe source (M1170) being in the center of the polyethylene cylinder. An isotropic, monoergic 2.45-MeV neutron source in the center of the polyethylene cylinder was the second case. Using ^{3}He neutron cross-sections obtained from the Brookhaven National Laboratory National Nuclear Data Center on-line access, MORSE provided, in each case, response functions for elastic scattering, (n,p), and (n,d) reactions at several locations in one of the six ^{3}He proportional counters. Calculation of the theoretical efficiency of one proportional counter for each case involved fitting the ^{3}He(n,p) responses with an appropriate analytic function, and integrating the function over the spatial limits of the proportional counter. Since the detector is azimuthally symmetric, the efficiency of the entire detector was found by multiplying the integrand by six. The contribution of elastic scattering and ^{3}He(n,d) reactions to detector efficiency were found to be two or more orders of magnitude less than the uncertainty in the measured efficiency. Details of these calculations can be found in Appendix A.

With knowledge of the theoretical efficiency for two cases, and a corrected measured efficiency, the estimated upper limit of efficiency of the detector, ϵ, for 2.45-MeV DD neutrons is then given by

$$\epsilon_{DD} = (Corrected\ measured\ \epsilon_{PuBe}) \left(\frac{Theoretical\ \epsilon_{DD}}{Theoretical\ \epsilon_{PuBe}} \right) \tag{4}$$

$$\epsilon_{DD} = (0.13) \frac{(0.72 \pm 0.07)}{(0.7 \pm 0.1)} = 0.134 \tag{5}$$

The theoretical efficiencies calculated by MORSE, as seen in equation (5), appear to be five to six times higher than the measured efficiency. This result is therefore somewhat questionable, but it was decided to use the ratio anyway, because it was the only tool available to estimate the efficiency of the detection system for a DD source.

Procedure.

The experimental procedure was divided into five phases:

1. Identification and cleaning of the Ti samples
2. Loading the Ti with deuterium
3. Background counts
4. Application of mechanical stress to the samples
5. Metallographic analysis.

This section discusses the five phases.

Identification and Cleaning. The first phase in the procedure was to identify and clean the Ti samples. The samples were cut from a 0.05-inch-thick sheet of commercially pure Ti (see Fig. 6). Each piece was engraved sequentially with a number, starting with the number one. The number was engraved, with a vibrating engraver, on each end of a sample, so both halves could be identified after the sample was stressed. The samples were then cleaned in the following sequence:

1. Cleaned with Cameo brand metal cleaner to remove printed marks and other macroscopic particles

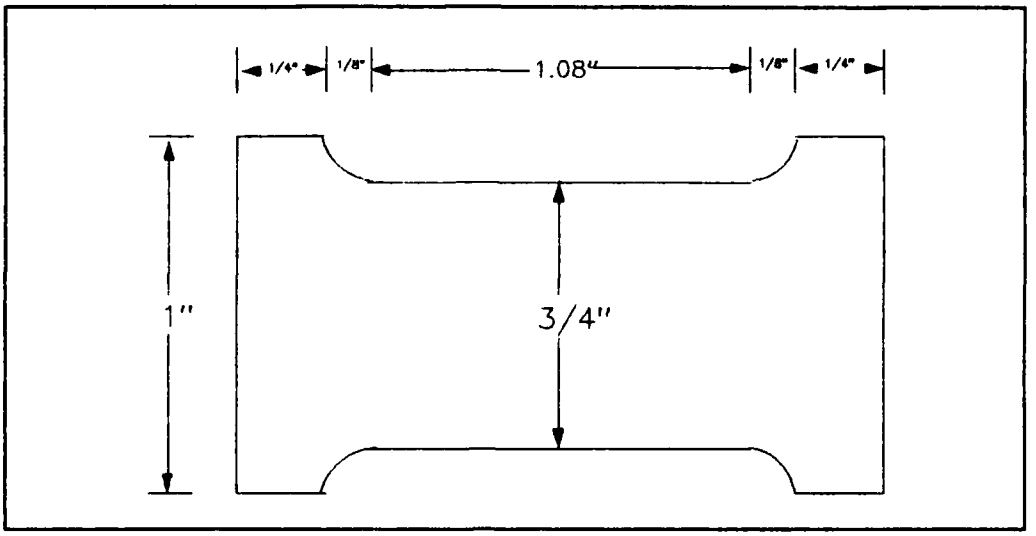

Fig. 6. Titanium Sample (0.05" Thick)

2. Placed in an ultrasonic cleaner that was filled with hot water, for at least five minutes, to remove Cameo residue. From this time, until placed in the grips for stress application, the samples were handled with tweezers to minimize any subsequent contamination.

3. Rinsed with deionized water

4. Placed in a beaker that contained a sufficient amount of acetone to completely cover the samples, and then the beaker was placed back in the ultrasonic cleaner for at least two minutes

5. After air drying, placed in a beaker that contained sufficient methanol to cover the samples, and then the beaker was placed back in the ultrasonic cleaner for at least two minutes

6. Allowed to air dry and then placed in a dessicator

Loading with Deuterium. Individual Ti samples were weighed and then inserted into a quartz chamber, and the quartz chamber was then attached to a vacuum manifold, with a total volume of 2540 ± 18 cm^3, so that one

of the broad sides of the sample faced the front of the vacuum system. An IR pyrometer was placed 18-20 inches in front of the vacuum system to measure the temperature of the sample.

After attaching the quartz chamber to the manifold, the diaphragm and molecular drag pumps were started to enable subsequent ion pump operation. Once the ion pump was running, the diaphragm and drag pumps were sealed off from the manifold, and the flange that connected the quartz chamber to the manifold was helium leak-checked.

Once the flange that connected the quartz chamber to the manifold was successfully leak-checked, the vacuum system was pumped down and then flushed twice with D_2 gas, to further dilute any contaminants that might remain in the system. The system reached pressures between 9.2×10^{-7} torr and 5.5×10^{-6} torr after leak-checking and before flushing. Table 1 shows details of the flushing process and an estimate of contaminant dilution for each sample.

Flushing was followed by a He leak-check of the valve separating the drag pump from the manifold and then by degassing of the sample. During degassing, samples were heated inductively to a temperature of 598 ±6°C. The samples were brought up to that temperature over a time span of about twenty minutes. After setting an initial power setting on the induction heater, system temperature and pressure were monitored. As temperature increased, outgassing started and the pressure increased. When the pressure stopped increasing, the power setting on the induction heater was increased. Initial power increases were in increments of 5-7 mA. Later power changes were in increments of 1 mA or less.

Table 1. Contaminant Dilution in Vacuum System

Sample No.	7	8	9	10
Pressure Before Flushing (torr)	4×10^{-6}	5.5×10^{-6}	1.8×10^{-6}	9.2×10^{-7}
First Flush Pressure (torr)	242	217.0	253.5	290.0
Post-Flush Pressure (torr)	$<1 \times 10^{-5}$	1.5×10^{-5}	7×10^{-6}	8×10^{-6}
Second Flush Pressure (torr)	735	310.5	215.8	201.6
Post-Flush Pressure (torr)	3×10^{-6}	5×10^{-6}	1.4×10^{-6}	2×10^{-6}
Contaminant Dilution(Est.)	9×10^{-25}	8×10^{-24}	4×10^{-25}	3×10^{-25}

Degassing continued until the pressure in the vacuum manifold decreased below 5 x 10-6 torr. When the pressure decreased below that value, the induction heater was turned off and the samples were allowed to cool.

Once the samples cooled back to room temperature, the temperature was recorded and the samples were loaded with deuterium. This was done by filling the manifold with D_2 gas to a pressure of 764 ± 3.7 torr, and then heating the samples inductively to a temperature of 643 ±4°C. The initial power setting on the induction heater was 60, which was equivalent to 32 mA. Inevitably, the temperature of the samples would overshoot the desired temperature, by as much as 14°C, but corrections were made so that the temperature of the samples was stable for the last half

of the loading process, which took 13-25 minutes. The induction heater was turned off when the manifold pressure dropped below 430 torr, and the samples were once again allowed to cool to room temperature.

After cooling, room temperature was recorded and the system was prepared for another sample. Preparation involved pumping out any D_2 gas remaining in the manifold and venting the system to air through a column of Drie-rite. Venting was followed by removal of the quartz chamber from the manifold and the exchange of a loaded sample for a new sample. The loaded sample was placed in a dessicator and the quartz chamber was immediately replaced on the manifold.

Background Counts. Before applying stress to any samples, I conducted two background counts at the location of the experimental trials and an investigation into the effects of external influences on the neutron detection system was made. A third background count was recorded after the first experimental trial. Data from the background counts were analyzed with a program called LABSTATS, which is written in Quick Basic and analyzes nuclear counting data. It also has an option that rejects data points more than three standard deviations away from the mean value. LABSTATS calculates standard statistical quantities such as the mean and standard deviation and runs Chi-square tests for Poisson and Normal distributions.

The first two background counts were made with the 4π detector in place in the Instron, and the grips were also in place for the first background count. The Instron had power on for the duration of the two

counts. Both counts were made with the MCA set to record 60 seconds/channel, and were started after the detection system had been warmed up about five minutes. The first count was made overnight, with a duration of 12 hours and 30 minutes. The second count was made over a weekend, with a duration of 37 hours and 44 minutes.

Both of the first two background counts showed that the neutron detection system was sensitive to overhead lights being turned on in the room. Whereas the typical count per channel overnight or during the weekend was in multiples of ten, hundreds or thousands of counts were recorded in individual channels while the lights were being turned on in the morning. The second set of measurements indicated that the neutron detection system required between 45 and 60 minutes to warm up and stop generating spurious counts.

The third set of background measurements was conducted for five minutes with the MCA set to record 0.4 seconds/channel. The 4π detector was not in the Instron, but standing several feet away, and the system had been warming up for several hours.

Application of Stress. This phase included the application of tensile and shear stresses to the samples. In either case, it began by insuring the neutron detection system was on and warming up for at least one hour prior to conducting an experimental trial. Turning the neutron detection system on for warmup included applying power to the NIM bin which contained the detection system's electronic modules and setting the operating bias of the ^{3}He proportional counters to 1200V.

Once the neutron detection system was warmed up, tensile stress was applied to one sample using the Instron, and to another sample with a static load of 50 pounds. More samples would have been stressed with the Instron except the deuterided titanium was so brittle that two samples out of three cracked while installing the neutron detector and gripping assembly in the testing machine.

In addition to tensile stress, the effect of shear stress on cold fusion was investigated. The shear stress was applied to two samples with a pair of $12\frac{1}{2}$-inch long household shears.

The first step in the application of tensile stress was to place the samples in a set of grips that were designed to fit inside the 4π neutron detector and connect to the Instron. I wore new non-sterile rubber gloves, from which all external dust had been removed, when taking the samples from the dessicator and placing them in the grips. As a further precaution to prevent contamination of the samples, the jaws of the grips were cleaned before being used the first time, the same way that the components of the vacuum system were cleaned.

The procedure for placing samples in the grips was dictated by the design of the grips and the brittleness of the deuterided titanium. When testing the grips before conducting experimental trials, it was found that the lower grip had a tendency to generate uneven pressure on non-deuterided samples and slip before the samples failed. To remedy this, I placed one half of a non-deuterided sample into the lower grip, narrow end first, before inserting the deuterided samples. On the other hand, deuterided titanium was extremely brittle and had a tendency to

break while being placed into the grips or while the grips and 4π detector were being moved into the Instron. Therefore, the grips were tightened using an allen wrench instead of a torque wrench, since the smallest available torque wrench, if set to its lowest setting, 100 inch-lbs, would have tightened the grips to the point of breaking the samples. With this in mind, the samples were placed in the lower grip first, to a depth of 3/16 inch, and the bolts were tightened with the long end of a 3/16 inch allen wrench inserted into the bolts. This left only the short end for leverage, and the bolts were tightened 1/2 turn past the point of increased resistance.

Following the tightening of the lower grip, the procedure depended on how tensile stress was being applied. When the Instron was used, then the sample was inserted immediately into the upper grip. For the application of the static load, the bolts in the lower grip were removed immediately after tightening, and only the jaws of the grip and the cylinder surrounding the jaws were retained. Then two six-foot lengths of 1/8 inch diameter wire with an exterior steel braid were inserted into the top of the surrounding cylinder so that the opposite ends of one wire were inserted into adjacent holes and the opposite ends of the other wire were inserted into the other two holes in the cylinder. After insertion of the wires, the sample was placed into the upper grip. In both cases,the samples were inserted to a depth of 3/16 inch into the upper grip. Only the short end of the allen wrench would fit between the grips, so the bolts in the upper grip were tightened 1/4 turn past the point of increased resistance.

Dynamic Stress. When using the Instron, the second step was to place the entire gripping assembly into the center of the 4π detector, roll the detector into place, in the Instron, and connect the grips to the Instron. The grips were designed so that the sample was held in the center of the polyethylene cylinder in the 4π detector.

The next step was to insure that recording devices were setup properly. The multi-channel analyzer (MCA) in the neutron detection system was operated in a multi-scale mode with 4096 channels, with a counting time of 0.4 seconds/channel. With a previously measured background of 12.5 ± 0.2 counts/minute, 0.4 seconds/channel insured that one count in a channel would be statistically significant (greater than three standard deviations above background) and maximize the sensitivity of the detection system. With the MCA set, an X-Y plotter that recorded Instron load vs. time was set up to record, with an X-axis time scale of 20 seconds/inch and a Y-axis full scale load of 10,000 pounds.

Application of stress was the final step. MCA acquisition was started, and then three minutes (channel 450) later, the Instron was started at a speed of 0.1 inches/minute. The X-Y plotter was started concurrently with the Instron. After failure of the sample, the Instron was turned off, the X-Y plotter reset, and the MCA acquisition was supposed to be stopped, and the data recorded.

Stress by Static Load. When applying tensile stress with a static load, the second step was to support the gripping assembly and wires in the 4π detector. This was done by placing two six-inch high vise grips on top of the detector, about 8 inches apart, opening the

vises 1/4 inch, and then supporting the upper grip on the vises with a 9-inch long, 3/8-inch diameter pin. The pin went through the 3/8-inch hole near the end of the grip's steel shaft and rested on top of the opening in the vise grips. This arrangement suspended the sample in the middle of the polyethylene cylinder in the 4π detector.

After the gripping assembly and wires were in place, two 25-pound weights were suspended from the wires. I initially supported the weights so they would place no load on the sample, looped the wires through the weights, and tied knots in the wires. With the support removed, the weights were gently lowered, without jerking the sample, until they were hanging freely.

With the weights hanging freely, the MCA was started in multi-scale mode with a setting of 1 second/channel. The time per channel was increased in order to facilitate analysis of the data from the MCA. When one count in a channel is statistically significant and rejected from background, the background is always found to be zero. A background of zero made it impossible to discern background events from possible cold fusion events, and with the new setting 2 counts in a channel was the statistically significant minimum. The MCA recorded neutron counts for a preset time of 1800 seconds.

Shear Stress. The last type of stress applied was shear stress. When applying shear stress, the MCA was started in multi-scale mode, recording 0.4 seconds/channel. I then placed a sample, or part of a sample, in the blades of the shears, applying just enough pressure to hold the sample in place. The shear and sample were then inserted in

the bottom of the 4π detector's central hole. This placed the sample 9 inches from the bottom of the detector, or 3 inches below the center of the polyethylene cylinder, which had the effect of introducing greater uncertainty into the estimate of neutron detector efficiency. One minute after starting the MCA, I sheared the sample and held the shears in the central hole for five seconds. Since the sheared pieces generally remained in the shears, some of the pieces remained in the detector for five seconds (channels 150-163).

Metallographic Analysis. Metallographic analysis was done for two reasons. The first reason was to characterize the Ti samples involved in the research. Characterization was done, in part, with optical metallography. The second reason was to obtain an estimate of the real area of a fracture surface. An estimate of the real area of a fracture surface can be used to calculate the number of atomic bonds broken in a fracture and provide a method of comparison with similar experiments. Imagery for the estimate (19) was obtained using a scanning electron microscope (SEM).

Optical Metallography. Characterization of the Ti samples was done with optical metallography. Two samples, one that had been cleaned but not loaded with deuterium, and one that was loaded with deuterium, were examined. The former sample was examined to find any visible hydrides already present and the volume fraction of β-phase Ti in the metal. Volume fraction of TiD_2 and precipitated deuterium were the features of interest in the latter sample. Both samples were cut so that two perpindicular planes of the metal could be viewed. Before grinding

and polishing, pieces from the clean, nondeuterided sample were mounted in Buehler Epomet Molding Compound and pieces from the deuterided sample were cold-mounted in Struers Epofix Resin.

Grinding and polishing followed a standard type of sequence. Grinding was done with 240, 320, 400, and 600 grit silicon carbide grinding papers, in sequence, on a rotary wheel. Intermediate polishing was then accomplished with 15, 9, and 6 micron diamond pastes, in sequence, on the back of a 5 x 8 index card. Buehler Mastermet, a 0.06-micron colloidal silica suspension, was used in a vibratory polisher for the final polishing.

Staining or etching of the various pieces followed the grinding and polishing. One piece from each sample was stained with a mixture of 10 ml KOH (40%), 5 ml H_2O_2, and 20 ml water. This mixture stains unalloyed α-phase Ti (20:141). The other piece from each sample was etched with a solution of 1 to 3 ml HF, 10 ml HNO_3, and 30 ml lactic acid. This etchant reveals hydrides (20:141) by preferentially etching non-hydrided Ti.

After staining or etching, the samples were viewed on optical metallographs, at magnifications up to 400X. Photographs (at 400X magnification) of representative fields including stained α-phase Ti or revealed deuterides were taken. Figure 7 is a photograph of the deuterided sample. The photos were analyzed later, using the techniques of quantitative stereology.

Fig. 7. Photograph of Deuterided Ti(400X)

Scanning Electron Microscopy. As mentioned in the beginning of this section, imagery for an estimate of the real area of a fracture surface was obtained via scanning electron microscopy. The fracture surface chosen for examination was from the sample that underwent tensile stress in the Instron.

Initial preparation of the sample was very similar to the preparation of the other samples for optical metallography. The sample was cut and cold-mounted so that two perpindicular profiles of the fracture

surface could be viewed. Grinding and polishing were done in the same manner as previously described, except the final polishing was of about 25 hours duration. The longer final polishing time was required because the cold-mounting material is softer than the Epomet mentioned before and tends to accumulate grit during intermediate polishing. The grit is then released during the first few hours of final polishing, which scratches the specimen and forces a longer final polishing time.

Final preparation of the sample was done by the technician in WRDC/MLLS who ran the SEM. The preparation was coating the polished surfaces with a layer of carbon approximately 150 angstroms thick, and attaching conductive strips to the mounted pieces for grounding purposes.

Once the mounted pieces from the sample were in the SEM, photographs were taken of the fracture surface and vicinity, with magnifications between 20X and 25000X. Some of the photos were used later to obtain an estimate of the actual surface area of the fracture.

IV. Results and Discussion

Deuterium Uptake in Samples

Table 2 shows the deuterium uptake of each sample and the trial(s) in which each sample was involved. An assumed density for Ti of 4.5 g/cm^3 was used in the calculations.

Table 2. Deuterium Uptake in Ti Samples

Sample #/ Trial	Initial Wt.(g)	Pressure Before Loading (torr±0.25)/ Temp.(°C)	Pressure After Loading (torr±0.18)/ Temp.(°C)	Atomic Percent D
7/Instron & Shear	5.97 ± 0.005	760.0/20.5	417.3/24.1	43.7 ± 0.43
8/Shear	5.93 ± 0.005	760.4/24.0	416.5/24.0	43.3 ± 0.44
9/ Metallography	5.85 ± 0.005	767.4/24.8	412.3/26.6	44.5 ± 0.43
10/Static Load	5.80891 ± 0.00003	760.3/26.2	390.8/26.5	45.4 ± 0.41

Application of Stress

Application of tensile stress with the Instron failed to generate any evidence of cold fusion. Analysis of the static load trial provided ambiguous indications of possible small neutron bursts. The shearing trials caused one burst to be recorded that might be of interest, but was probably caused by environmental effects.

As mentioned previously, turning on overhead lights affected the neutron detection system. Other environmental effects were noted. A flickering overhead light affected the detector. Banging the aluminum lining of the central 2.5 inch hole caused spurious counts and moving

the cables that connected to the ^{3}He proportional counters caused spurious counts. On the other hand, the system was insensitive to operation of the Instron and also to loud noises or banging on the outside of the 4π detector.

Dynamic Tensile Stress. When the Instron was used to apply tensile stress, the load peaked at 430 ± 15 pounds before the grips started to slip. The load decreased slowly during the slippage, but the sample failed at 50 ± 15 pounds of load about 95 ± 1 seconds after loading started. The data from the trial was lost when I forgot to stop data acquisition and store the data from the MCA. Before the data was lost, it was visible on a computer monitor and Dr. G. John, Capt P. Haaland, and I all agreed that no counts greater than background appeared to be visible.

Static Load Trial. The data from the static load trial was analyzed twice with LABSTATS, first rejecting statistically significant data points and then not rejecting them. The results were then compared with background. When analyzing the first two sets of background counts, LABSTATS rejected data points more than three standard deviations away from the mean of the data. The analysis of the third set of counts was done without rejection, because one count in a channel was rejected as statistically significant, which caused a calculation of a background count rate of zero. The average count rate and result of the Chi-square test for a Poisson distribution for the static load trial and each set of background counts is summarized in Table 3.

The result of the Chi-square test is interpreted as the probability that a random sample from a true Poisson distribution would have a greater variance from the predicted distribution than the sample being analyzed (21:126). If a probability greater than 0.95 or less than 0.05 is found, then equipment malfunction or an improper assumption of the governing distribution should be suspected. The Chi-square test results for the sets of background counts in Table 3 indicates that the neutron detection system probably operated properly.

Table 3. Results of Background Counts and Static Load Trial

Trial	T_{tot}**	T_c (s)*	Average Count Rate (s^{-1})	Chi-square	3σ Rejection (Y/N)	Fraction Rejected
Bkg. 1	12.5 hrs	60	0.209 ± 0.002	0.50<P<0.60	Y	0.01
Bkg. 2	37.75 hrs	60	0.197 ± 0.001	0.60<P<0.70	Y	0.01
Bkg. 3	5 min	0.4	0.18 ± 0.02	0.70<P<0.80	N	--
Static Load	30 min	1	0.153 ± 0.009	0.10<P<0.20	Y	0.02
Static Load	30 min	1	0.20 ± 0.01	0.01<P<0.02	N	--

**Total counting time
*Counting time per channel

Table 3 is useful for examining whether or not a low level of neutron emission was occurring in the sample during the trial. The count rate calculated with data point rejection is lower than that observed during background counts, and the count rate calculated without data

point rejection is in the middle or the range of observed background count rates. This would indicate that no detectable neutrons were being emitted, on average, during the trial.

I also compared the fraction of data points rejected as statistically significant to see if cold fusion neutron bursts could be identified that way. The fraction of data points rejected as statisticlly significant in the static load trial was twice that rejected during the sets of background counts. The distribution of counts in the static load trial also had much greater variance from a Poisson distribution than did the background, as indicated by the results of the Chi-square tests. This could be an indication of small bursts of neutrons from cold fusion. Thus, an average count rate approximately equal to background combined with statistics that indicate a large variance from the expected Poisson distribution, provide an ambiguous indication of possible cold fusion.

Since no detectable low-level neutron emission occurred, on average, during the trial, an upper level of neutron emission was estimated using the uncertainty in the average count rate, 0.01. As described earlier in this paper, the efficiency of the detector, ϵ, was estimated to be between 0.117 and 0.134. The sample used in the static load trial had absorbed 6.0687×10^{22} deuterium atoms. Therefore, the upper level of neutron emission is given by

$$Upper\ level\ {}_0^1n\ emission = \frac{(Uncertainty\ of\ ave.\ count\ rate)/\epsilon}{(Number\ of\ absorbed\ deuteron\ pairs)} \qquad (6)$$

In this case, the upper level of neutron emission is 1.2×10^{-24} neutrons per deuteron pair per second. This is an order of magnitude lower than the rate estimated by Jones (2:740).

Comparison with Jones' results, based on one data point, should not be taken as convincing evidence for or against cold fusion. It would require about 885 trials to verify Jones' result at the 95% confidence level. One trial provides only about a 50% confidence level. Appendix B shows the calculation of the number of trials required to obtain 95% confidence.

Shear Stress. During one of five trials of shear application, one channel (0.4 s/channel) recorded 2 counts. The other channels recorded 0 or 1 count and the five-minute background count conducted with 0.4 s/channel had no channels with 2 recorded counts. With an estimated detector efficiency of 0.117 to 0.134, 2 counts could indicate a burst of 15 to 17 neutrons. The burst could actually be larger, since the samples in these trials were not near the center of the ^{3}He proportional counters. What mitigates against calling this result positive is the relatively uncontrolled nature of these trials and the known sensitivity of the 4π detector to banging on the inner aluminum lining. Accidental contact with the lining could very easily have generated two counts.

Metallography

Optical Metallography. Analysis of the photographs from optical metallography was done with a technique from quantitative stereology. I placed a square grid, photocopied onto a transparent plastic sheet, over part of a photograph and counted the number of grid intersections that

overlapped a feature of interest in a photograph. The count was repeated over another part of the same photograph and then the average number of counted intersections was used to calculate the volume fraction of the feature of interest in the Ti sample.

The square grid was 50 mm on a side and had a pattern of 10 x 10 square boxes. This created 121 grid intersections, including corners and edges.

The number of grid intersections that lie over the feature of interest in a photograph is used to calculate a parameter known as the point count, P_p. Intersections that lie over the main part of the feature are counted once, while intersections that lie over the edge of the feature are counted as 1/2. The point count, P_p, for one measurement is defined as the number of counted intersections divided by the number of intersections in the grid (22:91). Assuming that multiple measurements represent the entire structure of the sample, the average point count for a series of measurements is related to the volume fraction, V_v, of the feature of interest by the relationship(22:92)

$$< P_p > = V_v \tag{7}$$

The results of the stereological analysis for the clean and deuterided Ti samples are in Table 4 below.

Table 4. Results of Optical Metallography

Sample	Clean	Deuterided
Feature of Interest	β-phase	TiD_2
V_v	0.25 ± 0.02	0.56 ± 0.02

In addition to finding the volume fractions as tabulated above, part of the purpose of the optical metallography was to identify visible hydrogen precipitate or hydrides in the clean sample and precipitated deuterium in the deuterided sample. No precipitated hydrogen or hydrides were visible in the clean sample, which indicates (See Fig. 1) a maximum hydrogen concentration in the clean sample of less than 1/2 atomic percent. Some specks of deuterium precipitate were visible in grain boundaries of the deuterided sample. However, they were too finely dispersed to measure quantitatively and do not appear to be scattered over more than 1/8 of the photographed area.

The implications of the optical metallography are three-fold. First, the clean sample did not have enough absorbed hydrogen to significantly inhibit deuterium absorbtion. Second, while some deuterium precipitate was visible in grain boundaries of the deuterided sample, the precipitate did not appear to provide large local concentrations of deuterium that might be conducive to cold fusion. Third, the volume fraction of TiD_2 in the deuterided sample provides another estimate of the deuterium uptake in the sample.

If it is assumed that the structure of the deuterided sample is either α-phase Ti saturated with deuterium ($\sim$0.5 at. %) or TiD_2, the concentration of deuterium in the sample can be estimated as

$$Conc(at.\ \%) = \left(V_{V_{TiD_2}}\right)(66.66) + \left(1 - V_{V_{TiD_2}}\right)(0.5) \qquad (8)$$

Substituting the value for volume fraction of TiD_2 from Table 4 yields

$$Conc(at.\ \%) = (0.56 \pm 0.02)(66.66) + (1 - (0.56 \pm 0.02))(0.5) = 38 \pm 5\% \qquad (9)$$

This value compares with a value of 44.5 ± 0.4 atomic % for this sample as shown before in Table 3. I attribute the difference between the two values to the difficulty in making an accurate count of grid intersections overlying the TiD_2, as the TiD_2 was well-dispersed throughout the sample.

Scanning Electron Microscopy. Two photomicrographs, one from each of the two photographed planes of the fracture surface, were selected for analysis. One photomicrograph (Fig. 8) had a magnification of 1000X, while the other was magnified by a factor of 2000X. These photomicrographs were selected because they were the highest magnification photos available that portrayed the fracture profiles across the full widths of the photos.

The fracture profile was used to calculate a parameter of the fracture surface known as the lineal roughness parameter, R_L (23:110). The lineal roughness parameter is defined by

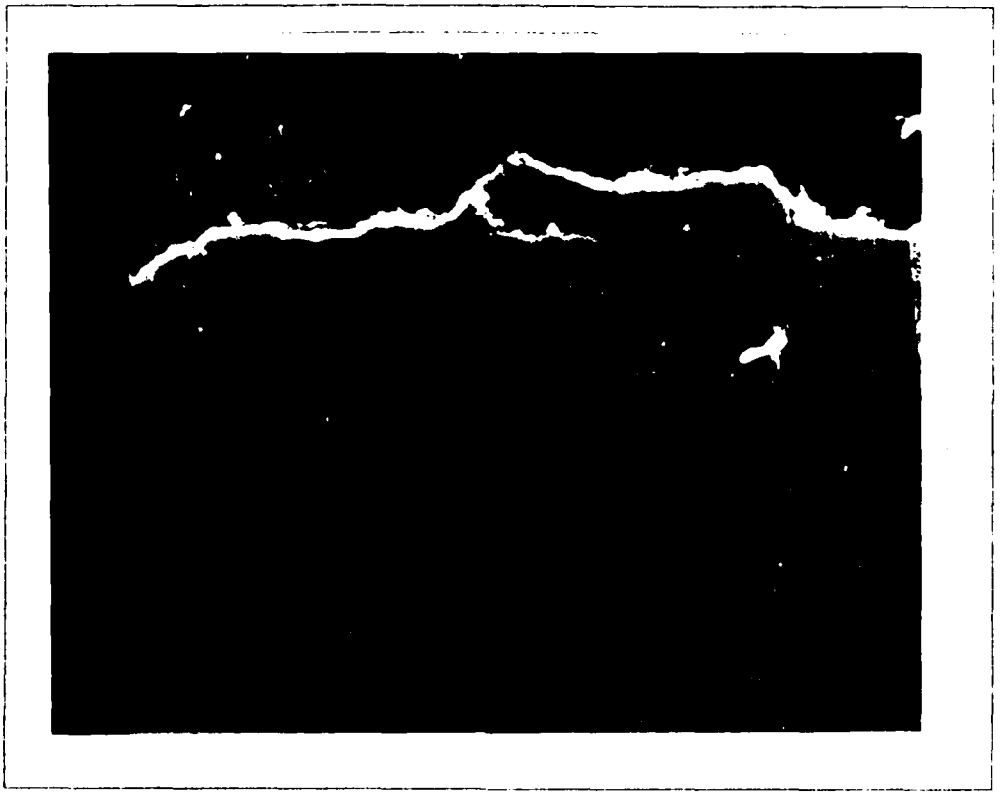

Fig. 8. Photomicrograph of Fracture Surface (1000X)

$$R_L = \frac{(True\ profile\ length)}{(Projected\ profile\ length)} \tag{10}$$

The true profile length is self-explanatory and the projected profile length is the measured straight-line length of the profile across the photomicrograph. Table 5 shows the results of these measurements for the selected photos.

Table 5. Lineal Roughness of Fracture Surface

Plane No.	1	2
Magnification	1000X	2000X
True Profile Length(cm)	10.1	11.3
Projected Profile Length(cm)	11.6 ± 0.2	12.9 ± 0.2
R_L	1.25 ± 0.02	1.14 ± 0.02
Average R_L	1.14 ± 0.01	

Once the average lineal roughness factor is known, an estimate of the actual fracture surface area can be made by multiplying the apparent surface area by R_l^2. The apparent fracture surface areas of the two samples were found after measuring the thickness of the samples with a micrometer and the length of the fracture surfaces with a piece of thread. Table 6 shows the results of these measurements and the estimates of the actual areas. These results assume the average R_L for the piece that underwent scanning electron microscopy is the average R_L for all of the fracture surfaces.

Knowledge of the samples' grain and crystalline structures can be combined with the estimate of the actual fracture area to estimate how many atomic bonds were broken as the samples were fractured. Under normal circumstances, titanium hydride tends to not have more H than $TiH_{1.73}$ (24:49). From Table 2, the average D concentration in samples 7 and 8 was 43.5 ± 0.3 atomic percent. If the TiD system behaves the same

Table 6. Areas of Fracture Surfaces

Sample No.	7	8
Length of Fracture Surfaces(cm)	17.1 ± 0.3	12.3 ± 0.3
Thickness(cm)	0.143 ± 0.001	0.146 ± 0.001
Apparent Area of Fracture Surfaces(cm^2)	2.4 ± 0.1	1.80 ± 0.08
Actual Area(cm^2)	2.9 ± 0.1	2.2 ± 0.1

as the TiH system, the average volume fraction of titanium deuteride in these samples was $0.68 \pm 2 \times 10^{-3}$. This result is easily obtained by solving an equation similar to (8) simultaneously with

$$V_{V_{\alpha\text{-}Ti}} + V_{V_{TiD_{1.73}}} = 1 \qquad (11)$$

The crystalline structures of titanium hydride and α-Ti yield values for the lattice constant, *a*. Titanium hydride is face-centered cubic or tetragonal, depending on temperature, but in either case *a* has a value of 4.5 ± 0.05 A(25:443). The lattice constant of α-Ti is 2.9511 ± 0.00005 A(25:1278).

If it is assumed that the D-saturated α-Ti is unexpanded beyond its normal lattice size, then the information from the preceding two paragraphs can be used to calculate the number of Ti atoms on the fracture surface. The end of the titanium hydride face-centered unit cell is square and the end of the α-Ti hexagonal-close-packed lattice can be viewed as one rhombus next to another rhombus. Therefore, in each case the area of the square or rhombus is a^2 and each square or rhombus contributes one Ti atom to the surface. Assuming each square centimeter of

surface had 0.68 cm^2 of titanium deuteride and 0.32 cm^2 of α-Ti exposed, on average, then each cm^2 of the samples had $7.03 \times 10^{14} \pm 5 \times 10^{12}$ Ti atoms/cm^2.

As each Ti atom on a fracture surface is presumed to have bonded with another Ti atom before the fracture occurred, the total number of atomic bonds broken in a sample was 1/2 the total number of Ti atoms on the fracture surfaces. It can therefore be estimated that $1.04 \times 10^{15} \pm 5 \times 10^{13}$ bonds were broken in sample number 7 and that $7.7 \times 10^{14} \pm 4 \times 10^{13}$ bonds were broken in sample number 8.

The fracture surface areas and, therefore, number of atomic bonds broken in this experiment can be compared with the results of H. O. Menlove, if some speculation is allowed. Menlove (4) used approximately 100 grams of Ti chips in his experiments. The chips were about 1 mm x 3 mm in size. If I speculate that the chips were also about 1 mm thick and that 1% of the chips fractured simultaneously at -30° C, the temperature at which Dolan(26:3) says Menlove reported most of his bursts, then I can estimate that roughly 4.4 cm^2 of apparent surface area was fractured at the time of the reported neutron bursts. This 4.4 cm^2 of apparent fracture surface area is comparable to the 4.2 cm^2 of total apparent fracture surface area in this experiment.

V. Conclusions and Recommendations

Two applications of tensile stress to deuterided titanium samples produced one ambiguous indication of cold fusion. Dynamic tensile stress generated no indications of cold fusion. On the other hand, a static load trial produced a low average count rate which would be a basis to reject the hypothesis that cold fusion occurred, but the variance of the measured count rate was much greater than expected for a Poisson distribution. One possible explanation of the large variance is cold fusion. The effect of shear stress on cold fusion was also investigated and generated what could be a positive result, but the result must be treated with skepticism because that part of the experiment was extremely sensitive to environmental factors. Therefore, I must tentatively conclude that mechanical stress, as applied in these trials, provided no positive evidence of cold fusion.

If there is interest in following up on this work, the application of tensile stress with a static load is the simplest experiment to perform and offers the greatest integration time in a single trial. Application of dynamic tensile stress with a materials testing machine is in some ways the most interesting method used, but the brittleness of the deuterided titanium must force a modification in procedure. Either the titanium must be deuterided to a much lesser extent(5 or so atomic percent), or the neutron detector must be redesigned, so the samples and grips can be attached to the Instron without having to initially be inside the detector. Application of shear stress would require a new experimental procedure.

Appendix A: Calculation of Efficiency of the 4π Detector

Table 7 contains the responses calculated by MORSE, for the ^{3}He(n,elastic scatter), ^{3}He(n,p), and ^{3}He(n,d) reactions in the 4π neutron detector. The response functions are given for several spatial locations in one ^{3}He proportional counter. The variable z refers to axial distance from the center of the ^{3}He tube.

Table 7. ^{3}He Response

Source and Reaction	z(cm)	Response $\left(\frac{barns}{^{3}He\ atom \cdot cm^{2} \cdot source\ n}\right)$	Fractional Standard Deviation
DD-Elastic	0.0	1.08×10^{-2}	0.0239
DD-Elastic	6.0	7.27×10^{-3}	0.0313
DD-Elastic	12.0	2.99×10^{-3}	0.0443
DD-(n,p)	0.0	10.2	0.0894
DD-(n,p)	6.0	8.8	0.0970
DD-(n,p)	12.0	4.7	0.1152
PuBe-Elastic	0.0	1.04×10^{-2}	0.03819
PuBe-Elastic	3.0	1.02×10^{-2}	0.03599
PuBe-Elastic	6.0	7.34×10^{-3}	0.02764
PuBe-Elastic	9.0	4.72×10^{-3}	0.03788
PuBe-Elastic	12.0	3.1×10^{-3}	0.08091
PuBe-Elastic	15.0	2.0×10^{-3}	0.06365
PuBe-(n,p)	0.0	9.0	0.10532
PuBe-(n,p)	3.0	8.0	0.06349
PuBe-(n,p)	6.0	8.2	0.07645
PuBe-(n,p)	9.0	6.6	0.10748
PuBe-(n,p)	12.0	4.5	0.17618
PuBe-(n,p)	15.0	3.5	0.15228
PuBe-(n,d)	0.0	3.92×10^{-5}	0.03616
PuBe-(n,d)	3.0	4.14×10^{-5}	0.02189
PuBe-(n,d)	6.0	2.47×10^{-5}	0.02357
PuBe-(n,d)	9.0	1.45×10^{-6}	0.03876
PuBe-(n,d)	12.0	7.45×10^{-6}	0.01389
PuBe-(n,d)	15.0	4.33×10^{-6}	0.03020

Efficiency for a DD Source

A least squares fit of the (n,p) response with a quadratic function was used to calculate the (n,p) efficiency for a DD source. The quadratic was of the form $y = a - bz^2$ and the following points were defined:

$z_0 = -12$
$z_1 = -6$
$z_2 = 0$
$z_3 = 6$
$z_4 = 12$

Then two more quantities were defined:

$$\epsilon_i = a - bz_i^2 - y_i \tag{12}$$

and

$$E = \sum_{i=0}^{4} \epsilon_i^2 = \sum_{i=0}^{4} (a - bz_i^2 - y_i)^2 \tag{13}$$

To minimize E, set

$$\frac{\partial E}{\partial a} = \sum_{i=0}^{4} 2(a - bz_i^2 - y_i) = 0 \tag{14}$$

and

$$\frac{\partial E}{\partial b} = \sum_{i=0}^{4} 2(a - bz_i^2 - y_i)(-x_i^2) = 0 \tag{15}$$

This yielded two simultaneous equations (The negative exponents of ten result from converting barns to cm^2):

$$10a - 720b = 7.425 \times 10^{-23} \tag{16}$$

$$-720a + 88128b = -3.9662352 \times 10^{-21}$$

The solution is then

$$(n,p)\ Response(z) = 1.01626 \times 10^{-23} - (3.80226 \times 10^{-26} z^2) \tag{17}$$

The (n,p) response for one tube is

$$(n,p)\ Response = \left(\frac{\#\ ^3He\ nuclei}{cm^3}\right)(\pi)(tube\ radius)^2 \int_{-15.24}^{15.24} (n,p)\ Response(z)\ dz \qquad (18)$$

The limits of integration in equation (18) are the length of the ^{3}He detector's sensitive volume. The tube radius is 1.27 cm^2 and at a pressure of 4 atmospheres, there are 1.0748 x 10^{20} He/cm^3 in the detector. Plugging these numbers and equation (11) into equation (12) yields an (n,p) response of 0.11986 reactions/source neutron/^{3}He tube.

I fit the elastic scattering response with a quartic interpolation in the region z = ± 12. Taking a forward difference approximation of the slope at z = -12 and taking advantage of the symmetry of the MORSE output, I assumed linear response functions outside of z = ± 12. However, the elastic scattering response of the ^{3}He proportional counter is two or three orders of magnitude lower than the (n,p) response. As a result, the result of integrating the elastic scattering response function affected the fifth decimal place of the total response function for one ^{3}He tube. The response from elastic scattering can therefore be considered insignificant.

Similarly, there is no (n,d) response for a DD source since the (n,d) reaction is endothermic and requires an input energy greater than 4 MeV.

Since the (n,p) response is the only significant component of the response of one ^{3}He proportional counter, the efficiency of the 4π detector for a DD source is six times the (n,p) response of one tube. This can be done because of the azimuthal symmetry of the detector. The efficiency of the 4π detector for a DD source is 0.72 ± 10% (based upon

F.S.D. of MORSE output).

Efficiency for a PuBe Source

The (n,p) response of the detector for a PuBe source was approximated with a least squares fit of a chopped cosine of the form $R(z) = a\cos\left(\frac{z}{b}\right)$. The process was parallel to that used to fit the response to a DD source, except the simultaneous equations had to be solved iteratively. The result of the least squares fit was

$$(n,p)\ Response(z) = 8.7065671 \times 10^{-24} \cos\left(\frac{z}{12.509814}\right) \qquad (19)$$

Integration of the response over the length of the ^{3}He proportional detector yielded a response of 0.11134 reactions/source neutron/^{3}He tube.

Once again, the (n,p) response was the only significant contribution to the response of the ^{3}He proportional counter. Elastic scattering response, as generated by MORSE was still 2 to 3 orders of magnitude lower, and the (n,d) response was 5 to 6 orders of magnitude lower. Therefore, the theoretical efficiency of the 4π detector for a PuBe source is 0.7 ± 15% (Refer to F.S.D. of MORSE output).

Deadtime Correction

The deadtime of a proportional detector can be used to estimate the true interaction rate inside a detector and is approximately equal to the charge collection time inside the detector. The charge collection time is dependent on the applied voltage, anode radius, cathode radius, and mobility of the positive ions and free electrons created by the

interaction of neutrons with the proportional gas. Mobility is dependent upon the mass of the charged particles, so the mobility of the heaviest positive ions must be used to determine the charge collection time.

Neutrons interact with ^3He in a $^3He(n,p)^3T$ reaction, so the heaviest positive ion produced in the ^3He proportional detector is tritium. The mobility of tritium in ^3He should be used to calculate the deadtime of the proportional detectors. Information on the mobility of tritium in ^3He was unavailable however, so the calculation of deadtime will use the mobility of ^4He ions in ^4He gas.

Three assumptions were made before calculating the deadtime. The first assumption was that the radius of the anode, a, is 0.005 cm. The cathode radius, b, was assumed to be 1.27 cm, which is the nominal outside radius of the ^3He proportional detectors, but all six of the detectors have outside radii at least 0.05 cm larger than nominal. Formation of positive ions was assumed to occur at the anode surface, which assured that an upper limit of the deadtime was calculated. Details of the calculation follow.

Calculation of the deadtime requires knowledge of the electric field magnitude in the detector. Since the applied voltage, V_b, was 1200 volts, the magnitude of the electric field inside the proportional counters can be calculated using the relationship (27:5-4)

$$|\vec{E}| = \frac{V_b}{\alpha \ln\left(\frac{b}{a}\right)} \tag{20}$$

Substituting the appropriate values into equation (20) yields

$$|\vec{E}| = \frac{1200V}{0.005\ cm\ \ln\left(\frac{1.27\ cm}{0.005\ cm}\right)} = 4.3x10^{4}\frac{V}{cm} \tag{21}$$

The magnitude of the elctric field ts multiplied by the mobility of the positive ions to obtain the drift velocity of the ions (27:5-4). $^{3}He^{+}$ has a mobility, μ of 6.16 $cm^2/V\text{-}s$ (28:111).

$$v^{+} = \mu|\vec{E}| = 2.6x10^{5}\frac{cm}{s} \tag{22}$$

Finally, the collection time is found to be

$$t_{coll} = \frac{b-a}{v^{+}} = 4.9x10^{-6}s \tag{23}$$

This value of the collection time is used as the deadtime when estimating the true interaction rate.

The relationship between measured count rate and true interaction rate for a paralyzable detector is (21:97-98):

$$m = ne^{-n\tau} \tag{24}$$

where

n = true interaction rate

m = measured count rate

τ = system dead time

Equation (24) can be solved to obtain the true interaction rate, which can then be used to calculate the efficiency of the detector for a situation where a low counting rate is expected. Modeling the detector as paralyzable was done because some output pulses from the linear amplifier were observed to have "shoulders" on their trailing edges.

The measured count rate during the measurement of detector efficiency was 1.44×10^{20} counts/s, and substitution of this value and the dead-time into equation (24) yields a true interaction rate of 1.6×10^{4} counts/s. Dividing the true interaction rate by the neutron production rate of the source used in this measurement, 1.23×10^{5} neutrons/s, yields a corrected measured efficiency of 0.13.

Appendix B: Calculation of Number of Trials Required to Obtain 95% Confidence Level

A confidence level is actually 1 minus the probability of making a type 1 error (29:15). A type 1 error occurs when a true hypothesis is rejected as false. To calculate the number of trials this requires, the following equation must be solved.

$$\frac{\overline{X}_c - X_d}{\sigma/\sqrt{n}} = Z_{confidencelevel} \tag{25}$$

where $\overline{X}_c$ is the critical value of X, X_d is the desired value of X, σ is one standard deviation, n is the number of trials, and Z is from the normal distribution (29:20). X_d and Z are known, and if σ can be estimated, then the equation has two unknowns left. Therefore, there must be another equation to solve simultaneously.

The second equation is provided by the need to calculate not only the confidence level, but also the probability of making a type 2 error. A type 2 error is accepting a false hypothesis as true (29:15). The second equation is then

$$\frac{\overline{X}_c - \overline{X}_o}{\sigma/\sqrt{n}} = Z_\beta \tag{26}$$

where $\overline{X}_o$ is the original average value of x, and β is the probability of making a type 2 error (29:20). Solution of equations (25) and (26) will yield a value for the number of trials and $\overline{X}_c$, the critical value above which a hypothesis should not be rejected as false.

To fill in these equations, $\overline{X}_o$ was taken to be the average count rate from the sets of background counts, and X_d was based upon Jones' results. Jones reported 4.1 x 10^{-3} counts/s above background using a detector with 1% efficiency. Muliplying his count rate by 12 and adding it to my background count rate gave a value of 0.2492 for X_d. The sample standard deviation of the count rate in the static trial was 0.5, and β was set equal to 0.1. The two equations then became

$$\frac{\overline{X}_c - 0.2492}{0.5/\sqrt{n}} = -1.645 \tag{27}$$

and

$$\frac{\overline{X}_c - 0.2}{0.5/\sqrt{n}} = 1.282 \tag{28}$$

The solution to these two equations is n = 885 and $\overline{X}_c$ = 0.22. Therefore, 885 trials would be required to achieve a 95% confidence level while maintaining a 90% chance of avoiding a type 2 error. Also, any trial with an average count rate greater than or equal to 0.22 counts/s should not be rejected as evidence of cold fusion.

Bibliography

1. Fleischmann, Martin and Pons, Stanley. "Electrochemically Induced Nuclear Fusion of Deuterium," Journal of Electroanalytical Chemistry and Interfacial Electrochemistry, 261: 301-308 (1989).

2. Jones, S.E., et al.. "Observation of Cold Nuclear Fusion in Condensed Matter," Nature, 338: 737-740 (1989).

3. Bridgman, Charles J. The Physics of Nuclear Explosives, Chapter 4, AFIT Class Notes, NENG 605, School of Engineering, Air Force Institute of Technology(AU), Wright-Patterson AFB, OH, March 1988.

4. Menlove, H. O. Los Alamos National Laboratory. Telephone Interview. 15 August 1989.

5. DeNinno, A., et al.. "Evidence of Emission of Neutrons From a Titanium-Deuterium System," Europhysics Letters, 9: 221-224 (1989).

6. Caskey, G.R., Jr. "The Influence of a Surface Oxide Film on Hydriding of Titanium," Conference on the Effects of Hydrogen on Materials Properties and Selection and Structural Design. 465-474. Metals Park, OH: American Society for Metals, 1974.

7. Thaddeus, E. and B. Massalski. Binary Alloy Phase Diagrams, Volume 2, Metals Park, OH: American Society for Metals, 1986.

8. Gittus, John and James Bockris. "Explanations of Cold Fusion," (Scientific Correspondence) Nature, 339: 105 (1989).

9. Margolin, Harold. "Stress, Hydrogen Segregation, and Fracture in α-β Titanium Alloys," Metallurgical Transactions A, 7A: 1233-1235 (1976).

10. Paton, N. E. and J. C. Williams. "Effect of Hydrogen on Titanium and its Alloys," Conference on the Effects of Hydrogen on Materials Properties and Selection and Structural Design. 409-431. Metals Park, OH: American Society for Metals, 1974.

11. F. J. Mayer, et al.. "Nuclear Fusion from Crack-Generated Particle Acceleration," Highlights of Papers Presented at the Workshop on Cold Fusion Phenomena. LA-11686-C. 25. Santa Fe: Los Alamos National Laboratory, 1989.

12. Walter G. Cady. Piezoelectricity. Volume 1, New York: Dover, 1964.

13. B. V. Derjaguin, et al.. "Titanium Fracture Yields Neutrons?" (Scientific Correspondence) Nature, 341: 492 (1989).

14. Jordan, Edward C. and Keith G. Balmain. Electromagnetic Waves and Radiating Systems. (Second Edition). Englewood Cliffs, NJ: Prentice-Hall, 1968.

15. X-ray fluoresence analysis performed at Air Force Materials Lab, WRDC/MLSA.

16. Lenning, G. A. and R. I. Jaffee. Effect of Hydrogen on the Properties of Titanium and Titanium Alloys, Columbus, OH: Battelle Memorial Institute, December 1955. (AD-82738).

17. Macklin, R.J., et al.. "Neutron Multiplicity Counter," Nuclear Instruments and Methods, 102: 181-187 (1972).

18. Emmett, M.B. "The MORSE Monte Carlo Radiation Transport Code System," ORNL-4792(February 1975); ORNL-4972/R1(February 1983); ORNL-4972/R2(July 1984). Work performed by Major D. Beller, AFIT/ENP.

19. Scanning electron microscopy performed at Air Force Materials Lab, WRDC/MLLS.

20. Metals Handbook, Volume 8, (Eigth Edition). Metals Park, OH: American Society for Metals, 1961.

21. Knoll, Glenn F. Radiation Detection and Measurement. New York: John Wiley and Sons, 1979.

22. DeHoff, R. T. "Problem Solving Using Quantitative Stereology," Applied Metallography. Edited by George F. Vander Voort. New York: Van Nostrand Reinhold, 1986.

23. Underwood, Ervin E. "Quantitative Fractography," Applied Metallography. Edited by George F. Vander Voort. New York: Van Nostrand Reinhold, 1986.

24. Molchanova, E. K. Phase Diagrams of Titanium Alloys. Israel Program for Scientific Translations Ltd., 1965.

25. Pearson, William B. A Handbook of Lattice Spacings and Structures of Metals and Alloys. New York: Pergamon Press, 1967.

26. Dolan, T. J. University of Missouri-Rolla. Handout from a "Minicourse on Aneutronic Fusion." Knoxville, Tn, 2 October 1989.

27. John, George. Nucleonics Instrumentation, AFIT Class Notes, NENG 650, School of Engineering, Air Force Institute of Technology(AU), Wright-Patterson AFB, OH, Spring 1989.

28. International Critical Tables of Numerical Data, Physics, Chemistry, and Technology. New York: McGraw-Hill, 1929.

29. Hicks, Charles R. Fundamental Concepts in the Design of Experiments. New York: Holt, Rinehart, and Winston, 1973.

UNCLASSIFIED
SECURITY CLASSIFICATION OF THIS PAGE

REPORT DOCUMENTATION PAGE

Form Approved
OMB No. 0704-0188

1a. REPORT SECURITY CLASSIFICATION UNCLASSIFIED	1b. RESTRICTIVE MARKINGS
2a. SECURITY CLASSIFICATION AUTHORITY	3. DISTRIBUTION / AVAILABILITY OF REPORT Approved for public release; distribution unlimited
2b. DECLASSIFICATION / DOWNGRADING SCHEDULE	
4. PERFORMING ORGANIZATION REPORT NUMBER(S) AFIT/GNE/ENP/90M-8	5. MONITORING ORGANIZATION REPORT NUMBER(S)
6a. NAME OF PERFORMING ORGANIZATION School of Engineering 6b. OFFICE SYMBOL (If applicable) AFIT/ENP	7a. NAME OF MONITORING ORGANIZATION
6c. ADDRESS (City, State, and ZIP Code)	7b. ADDRESS (City, State, and ZIP Code)
8a. NAME OF FUNDING / SPONSORING ORGANIZATION 8b. OFFICE SYMBOL (If applicable)	9. PROCUREMENT INSTRUMENT IDENTIFICATION NUMBER
8c. ADDRESS (City, State, and ZIP Code)	10. SOURCE OF FUNDING NUMBERS PROGRAM ELEMENT NO. / PROJECT NO. / TASK NO / WORK UNIT ACCESSION NO.
11. TITLE (Include Security Classification) INVESTIGATION OF THE EFFECT OF MECHANICAL STRESS ON COLD FUSION	
12. PERSONAL AUTHOR(S) Barton H. Wohl, Maj, USAF	
13a. TYPE OF REPORT MS Thesis 13b. TIME COVERED FROM _____ TO _____ 14. DATE OF REPORT (Year, Month, Day) March 1990 15. PAGE COUNT 68	
16. SUPPLEMENTARY NOTATION	

17. COSATI CODES			18. SUBJECT TERMS (Continue on reverse if necessary and identify by block number)
FIELD	GROUP	SUB-GROUP	
20	08		Deuterium, Thermonuclear Reactions, Neutron Detectors, Titanium
11	06	01	

19. ABSTRACT (Continue on reverse if necessary and identify by block number)

Thesis Advisor: George John
Professor of Nuclear Engineering
Department of Engineering Physics

20. DISTRIBUTION / AVAILABILITY OF ABSTRACT ☒ UNCLASSIFIED/UNLIMITED ☐ SAME AS RPT. ☐ DTIC USERS	21. ABSTRACT SECURITY CLASSIFICATION UNCLASSIFIED
22a. NAME OF RESPONSIBLE INDIVIDUAL George John, Professor	22b. TELEPHONE (Include Area Code) (513)255-4498 22c. OFFICE SYMBOL ENP

DD Form 1473, JUN 86 *Previous editions are obsolete.*

SECURITY CLASSIFICATION OF THIS PAGE
UNCLASSIFIED

The purpose of this research was to see if the phenomenon known as "cold fusion" could be observed after loading a sample of titanium with deuterium gas and then subjecting the sample to mechanical stress. Samples of commercially pure titanium were loaded with deuterium by heating them inductively to 643 ± 4° C while they were in a deuterium atmosphere. After loading, the samples were subjected to either dynamic tensile stress, a static load, or shear stress. The samples were surrounded by a 4-pi neutron detector during the application of stress and data from the detection system was analyzed for either large bursts of neutrons or continuous low-level emission of neutrons. Despite the fact that the neutron detection system was sensitive to certain environmental factors, application of tensile stress caused no positive indications of cold fusion. One suspiciously large count did occur during the application of shear stress, but that part of the experiment was relatively uncontrolled, and it is believed that the one large count was caused by environmental factors. An upper limit of 1.2×10^{-24} neutrons/deuteron pair/s has been calculated for the samples involved in this research. This is based on the limits of sensitivity of the neutron detection system.